<제 9회 KAI 항공우주 논문상 공모전 – 논문 요약본>

Assessment of CFD/CSD Coupled Aeroelastic Analysis Solution for HART II Rotor Incorporating Fuselage Effects

Young-Hyun You and Jeong-Hwan Sa

1. Introduction

The present work is an extension of the authors' previous works. The major goal of this research is to understand the physical mechanism leading to an improved prediction on airloads by incorporating a fuselage, as observed by Lim and Dimanlig. To this end, a loosely-coupled CFD/CSD algorithm is adopted to obtain a high resolution airloads solution. The distribution of induced velocity along with vorticity for a region of interest is obtained to support the present investigation. In addition, a vortex is traced all along from the formation to the final interaction with a blade. At the time of an interaction, the miss distance between the vortex and a blade has also been identified in the two models. Based on the observations, several important conclusions are made.

2. CFD/CSD Coupled Analysis

Both the comprehensive dynamics analysis system CAMRAD II [13] and a three-dimensional compressible flow solver KFLOW [14] are loosely-coupled to analyze the HART II rotor. The modeling details are described in this section. The KFLOW is a parallelized multi-block, structured, three-dimensional Navier-Stokes solver and is capable of computing time-accurate moving body problems by employing a Chimera overlapped grid system. The CAMRAD II is a comprehensive aeromechanical analysis system that is characterized by multibody dynamics, nonlinear finite elements, and various level of rotorcraft aerodynamic models.

A loose coupling alogorithm is applied to systematically combine the CAMRAD II (CSD) and KFLOW (CFD) codes. The key feature of the coupling is to exchange information between CFD and CSD codes on per revolution base.

3. Results and Discussions

The three test conditions of the HART II rotor such as the baseline (BL), minimum noise (MN), and minimum vibration (MV) cases are considered. The HART II rotor was in descent flight condition with an advance ratio $\mu = 0.15$, a hover tip Mach number $M = 0.6387$, and a thrust level $C_T = 0.00457$.

Figure 1 shows the comparison of the section normal force coefficient and pitching moment coefficient at 87% blade radial station for the BL case of the HART II rotor. It is seen that a good correlation is achieved with the present models against the measured data. In general, the predicted results with a rotor-fuselage model improve the correlation significantly, especially the high frequency airloads signals in the advancing and retreating sides of the rotor.

Figure 2 shows the iso-surfaces of Q-criterion colored by vorticity for the isolated rotor and rotor-fuselage models, when the reference blade is located at 32^{o} azimuth angles. The 32^{o} angle is selected since BVI peaks obtained from the two models differ significantly at this angle. As is demonstrated in the plots, the wake structure of the rotor is clearly visible. The region of interest near the tip (87% radial station) of the blade is denoted as a dotted circle for differentiation purpose. It is observed that nearly parallel tip vortices being about two and half revolutions old are approaching toward the reference blade which is rotating at the nominal RPM. The rotor-fuselage model presents more clear indication of encountering vortices with a blade at interest, as inferred from the previous results.

In Figure 3, the distribution of section normal forces M^2C_n obtained either from an isolated rotor model or a rotor-fuselage model over the entire rotor disk is presented, as a contour format. The flow is coming from the left and the rotation is made in the counter-clockwise direction viewed from the top. The overall loading patterns are seen to be essentially similar between the two models. However, two notable differences are observed: (1) the first quadrant of the rotor disk from the rotor-fuselage model predicts more oscillatory peaks; (2) near the front disk area of the rotor-fuselage model shows higher loading values than the isolated rotor case.

To understand the higher loading patterns due to the inclusion of a fuselage, the distribution of induced velocity field needs to be identified. The induced velocity profile is computed along the fore-aft (longitudinal) axis with the reference blade located at 20^{o} azimuth position. It is noted that the fore-aft axis is based from the hub plane and placed one chord length below the rotor disk. This lower position from the rotor disk allows avoiding the tip vortex regions where significant fluctuations of loadings will be experienced, but the flow patterns after the fuselage are influenced in a large scale by the wake of a body.

Figure 4 shows the comparison of induced velocity profile predicted along the longitudinal axis of the rotor. Both models show upwash in the front disk region of the rotor. It is indicated, however, that the upwash prevails all over the front disk area for a rotor-fuselage model while it is confined to parts of the disk for an isolated rotor model. The rear part of the disk shows downwash in both models, though highly oscillating pattern is observed with a fuselage. It is clear from the induced velocity distribution that the stronger upwash, induced due to a fuselage, is responsible to lift up a vortex at interest with a fuselage. The stronger upwash will also increase the local angle of attack, which essentially leads to higher lift forces. It should be mentioned that the change of inflow distributions in the fore-aft direction of a rotor affects on the lateral cyclic trim angles as well as on the tip path plane tilt angle. This will lead to a change in flap deflections. It is noted that the change of lateral trim angles between the isolated rotor and rotor-fuselage models is about 0.25^{o} for the BL case.

4. Conclusions

In this work, a loose coupling approach between CAMRAD II (CSD) and KFLOW (CFD) codes was employed to validate the HART II results for the BL, MN, and MV cases. The effects of a fuselage were investigated using both an isolated rotor and a rotor-fuselage model. The following conclusions were drawn from the investigation: (1) The predicted results on section aerodynamic loadings, BVI airloads, and blade elastic motions showed good agreements, as compared with the measured data. In general, a better correlation was obtained with a rotor- fuselage model. With the incorporation of a fuselage, the BVI signals in the advancing and retreating sides of the rotor disk were accurately captured and the phase error in the front disk area became corrected significantly. (2) The trajectory of a vortex at interest was traced from the formation to a final interaction. It was found that a vortex at interest was constantly shifting upwards until the interaction with a blade occurred. At the time of interaction, the miss distance was significantly reduced, leading to a stronger BVI phenomenon for a rotor- fuselage model. (3) The change in the induced velocity profiles due to a fuselage was quantified. The upwash patterns of a rotor-fuselage model showed stronger intensities with larger disk area, as compared with an isolated rotor model. It was observed that the higher upwash, induced due to a fuselage, was responsible to lift up a vortex at interest. The stronger upwash also affected on the higher loading near the front disk area as well as cyclic trim angles and blade deformations.

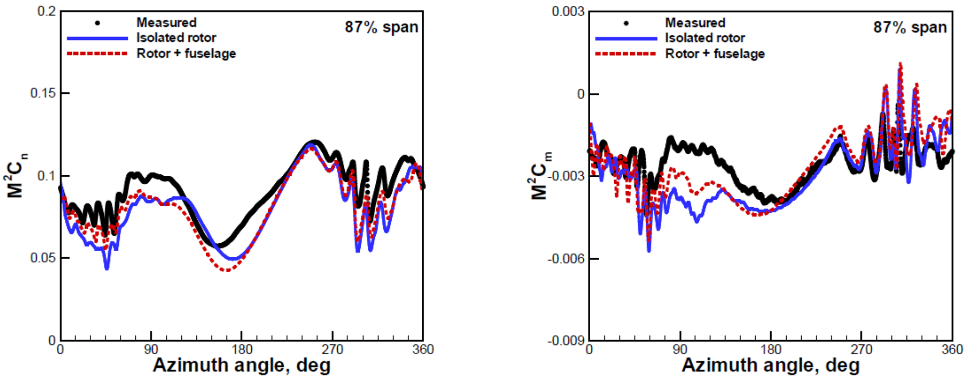

(a) Section normal forces **(b) Section pitching moments**

Fig. 1 Comparison of section normal forces and pitching moments at 87% radial location for HART II BL case.

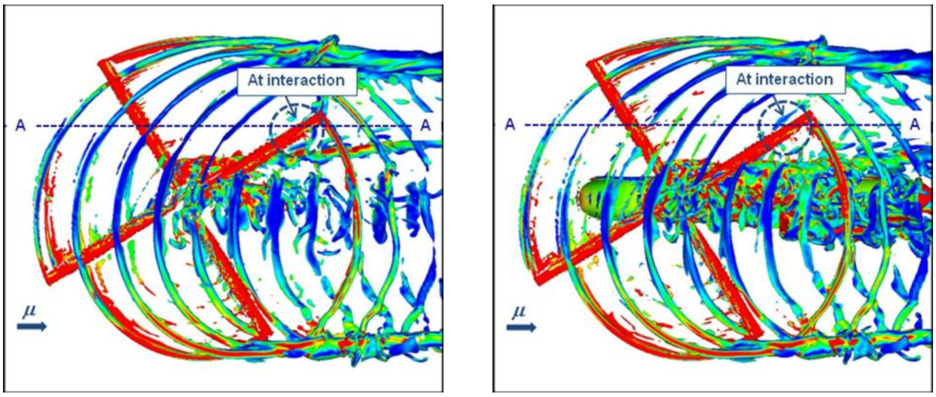

(a) Isolated rotor case **(b) Rotor-fuselage case**

Fig. 2 Comparison of iso-surfaces of Q-criterion colored by vorticity with locating the reference blade at 32° azimuth for the HART II BL case.

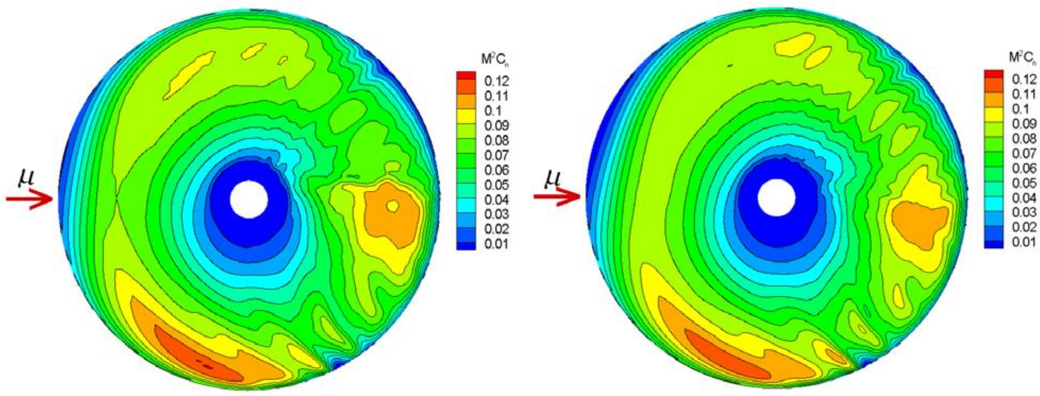

(a) Isolated rotor case **(b) Rotor-fuselage case**

Fig. 3 Comparison of contour plots for the section normal forces of HART II BL case.

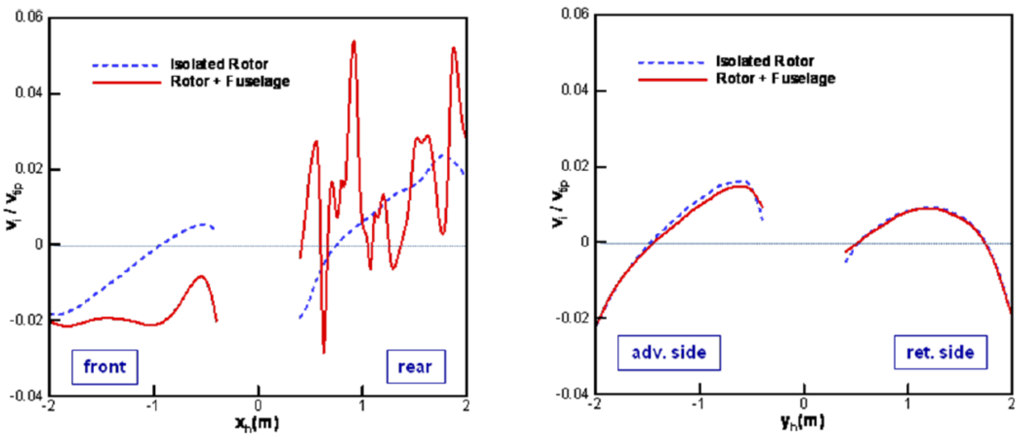

(a) Longitudinal distribution **(b) Lateral distribution**

Fig. 4 Comparison of induced velocity profiles at one chord length below of the hub plane (BL case).